



ELSEVIER

Available online at [www.sciencedirect.com](http://www.sciencedirect.com)

SCIENCE @ DIRECT®

Journal of Computational Physics 191 (2003) 249–264

JOURNAL OF  
COMPUTATIONAL  
PHYSICS

[www.elsevier.com/locate/jcp](http://www.elsevier.com/locate/jcp)

# De-aliasing on non-uniform grids: algorithms and applications

Robert M. Kirby <sup>a,\*</sup>, George Em Karniadakis <sup>b</sup>

<sup>a</sup> School of Computing, University of Utah, 50 S. Central Campus Drive, Salt Lake City, UT 84124, USA

<sup>b</sup> Division of Applied Mathematics, Brown University, Providence, RI 02912, USA

Received 7 January 2003; received in revised form 22 April 2003; accepted 23 May 2003

## Abstract

We present de-aliasing rules to be used when evaluating non-linear terms with polynomial spectral methods on non-uniform grids analogous to the de-aliasing rules used in Fourier spectral methods. They are based upon the idea of *super-collocation* followed by a Galerkin projection of the non-linear terms. We demonstrate through numerical simulation that both accuracy and stability can be greatly enhanced through the use of this approach. We begin by deriving from the numerical quadrature rules used by Galerkin-type projection methods the number of quadrature points and weights needed for quadratic and cubic non-linearities. We then present a systematic study of the effects of super-collocation when using both a *continuous Galerkin* and a *discontinuous Galerkin* method to solve the one-dimensional viscous Burgers equation. We conclude by examining three direct numerical simulation flow examples: incompressible turbulent flow in a triangular duct, incompressible turbulent flow in a channel at  $Re_\tau = 395$ , and compressible flow past a pitching airfoil at  $Re = 45,000$ .

© 2003 Elsevier B.V. All rights reserved.

## 1. Introduction

In spectral methods the quadratic non-linearities in the incompressible Navier–Stokes equations or the cubic non-linearities in the compressible Navier–Stokes are computed in the physical space. Specifically, the primary fields (i.e., velocity, pressure, energy) are first transformed into physical space, and subsequently the products are obtained at all quadrature points in a collocation fashion. Another transform is then performed to project the results back to modal space. More specifically, when the number of quadrature points  $Q$  is the same as the number of modes in the spectral expansion  $P$  we have a true collocation method, otherwise for  $Q > P$  we have a *super-collocation method*.

Errors may be caused by insufficient quadrature used in the Galerkin discretization of the non-linear terms, especially in complex-geometry flows [1]. Theoretical results in [2] provide a minimum requirement for the precision of numerical quadrature when computing volume and boundary integrals in the

\* Corresponding author. Tel.: +1-801-585-3421; fax: +1-801-585-6513.

E-mail addresses: [kirby@sci.utah.edu](mailto:kirby@sci.utah.edu) (R.M. Kirby), [gk@cfm.brown.edu](mailto:gk@cfm.brown.edu) (G.E. Karniadakis).

discontinuous Galerkin method. This result provides only a necessary condition on the number of quadrature points used. The errors caused by insufficient quadrature can be bounded by the theoretical estimates in [3], and quite often this result is used to support the idea that if the simulation is well-resolved, then the numerical crimes committed by insufficient quadrature are negligible. As was pointed out in [4], however, this does not address what happens in the marginally resolved simulation, which is far more often the case than most are willing to admit. Studies have also been performed to understand the effect of over-integration on accuracy when curvature is employed (see [5,6]). In the case of curved elements, the elemental mapping contains a non-constant Jacobian term within the elemental inner-product. The quadrature rules used for evaluating the inner-product must take the variable Jacobian into account when tabulating the quadrature order to be employed [7,8]. These studies, however, do not directly address the effect the choice of quadrature order used in the integration of the non-linear terms has on the stability of the solution. We propose that what are effectively polynomial aliasing errors can be eliminated and hence stability can be enhanced by employing over-integration, i.e., integrating the non-linear terms in the variational statement with higher order quadrature than the one employed for the linear contributions, e.g., pressure and viscous terms in an incompressible flow simulation.

This paper is divided as follows. We begin by deriving from the numerical quadrature rules used by Galerkin-type projection methods the number of quadrature points and weights needed for various orders of non-linearities. We demonstrate with a very simple computational example the ramifications of projection employing the standard number of quadrature points used for evaluating the inner product of the linear terms versus employing over-integration for the projections. We then present a series of studies in which we solve the one-dimensional *viscous* Burgers equation using both the continuous Galerkin and the discontinuous Galerkin methods. Discontinuous Galerkin solutions of the *inviscid* Burgers equation with and without over-integration are also examined. We then demonstrate the effects of over-integration through three direct numerical simulation examples: incompressible turbulent flow in a triangular duct, incompressible turbulent flow in a channel at  $Re_\tau = 395$ , and compressible flow past a pitching airfoil at  $Re = 45,000$ . We conclude by summarizing our findings and presenting general de-aliasing rules for polynomial spectral methods on non-uniform grids.

## 2. Accuracy, stability and over-integration

The following numerical quadrature rule for Gauss–Lobatto–Legendre quadrature is known (see [1]): Given  $Q$  quadrature points and corresponding weights (we will assume from hence forth that whenever referring to the number of quadrature points we also are referring to the corresponding weights), we can integrate a polynomial  $u(\xi) \in P_{2Q-3}$  exactly (to within machine precision computationally). From this rule we can compute for any given polynomial  $u(\xi) \in P_N$  the number of quadrature points  $Q$  as a function of  $N$  necessary for the quadrature to be exact. In Table 1 we present the number of quadrature points necessary given the polynomial order of the integrand for functions in  $P_N$ ,  $P_{2N}$ ,  $P_{3N}$ , and  $P_{4N}$ .

Table 1

Number of quadrature points necessary for Gauss–Lobatto–Legendre quadrature to be exact for given polynomial orders of the integrand

Polynomial order $N$	Number of quadrature points $Q$
$u(\xi) \in P_N$	$Q = \lceil (N + 3)/2 \rceil$
$u(\xi) \in P_{2N}$	$Q = \lceil (2N + 3)/2 \rceil$
$u(\xi) \in P_{3N}$	$Q = \lceil (3N + 3)/2 \rceil$
$u(\xi) \in P_{4N}$	$Q = \lceil (4N + 3)/2 \rceil$

In Galerkin methods, it is often the case that we are interested in computing numerically the inner product of two polynomials of the same (or lesser) degree, i.e., the inner product  $(\phi_i, \phi_j)$ , where  $\phi_i, \phi_j \in P_N$ . A polynomial of degree at most  $N$  has at most  $M = N + 1$  modal coefficients in its expansion. We can thus compute the number of quadrature points  $Q$  as a function of  $M$  necessary to integrate multiple powers of  $u(\xi) \in P_N$  exactly. In Table 2 we present the number of quadrature points necessary as a function of  $M$  given the polynomial order of the integrand for polynomials in  $P_{2N}$ ,  $P_{3N}$ , and  $P_{4N}$ .

From Table 2 we see that for linear problems which need only the inner product of two polynomials of the same or lesser degree (such as solving for the viscous terms of the incompressible Navier–Stokes equations using the continuous Galerkin method), only  $M + 1$  quadrature points are needed to integrate the inner product exactly. In the case of quadratic non-linearities, such as the convective contributions in the incompressible Navier–Stokes equations,  $3M/2$  points are needed. For cubic non-linearities, such as those found in the compressible Navier–Stokes equations,  $2M$  points are needed for the numerical integrations to be exact.

Most numerical solvers, however, only use the number of quadrature points necessary to integrate the linear terms exactly. To understand the ramifications of this “under-integration” of non-linear terms, we perform the following test:

- (i) Consider a single element in the space interval  $[-1, 1]$  containing  $M = 16$  Jacobi modes.
- (ii) Initialize all the modal coefficients to one.
- (iii) Evaluate the modal representation on a set of  $Q$  quadrature points.
- (iv) Square (in a pointwise fashion) the values at the quadrature points.
- (v) Pre-multiply the set of points (as a vector) by the collocation derivative matrix of the appropriate size (rank  $Q \times Q$ ).
- (vi) Project back to modal coefficients by discrete inner products using Gaussian integration.

The procedure above mimics the “physical space” or pseudo-spectral evaluation of the term  $\partial u^2 / \partial x$  commonly used in spectral methods for evaluating non-linear terms. This test was chosen because even in its simplicity it models the order of non-linearity that occurs in the solution of the incompressible Navier–Stokes equations. All modes are set to *one* to mimic a case in which an element has under-resolved or marginally resolved the solution within the element. In the test above, the only unspecified parameter is the number of quadrature points  $Q$  to be used. In using Gauss–Lobatto–Legendre points, the value of  $Q$  is taken to be one more than the number of modes  $M$  (in this case then  $M = 16$  and  $Q = 17$ ) [8], but this value is appropriate for the inner products corresponding to linear terms. For quadratic or cubic non-linearities more quadrature points are required as discussed previously. The ramifications of under-integration of this form are shown in Fig. 1. The figure on the left was obtained for a quadratic non-linearity  $((\partial/\partial x)u^2)$  and the figure on the right was obtained for a cubic non-linearity  $((\partial/\partial x)u^3)$ . The difference in the modal coefficients at the conclusion of the algorithm above for different values of  $Q$  is provided. We observe that for the quadratic non-linearity, once  $3M/2$  quadrature points are used the differences in the modal values do not change. Similarly for the cubic non-linearity, once  $2M$  quadrature points are used the differences in the modal values do not change. If instead of  $2M$  quadrature points for the cubic non-linearity  $3M/2$

Table 2  
Number of quadrature points necessary for Gauss–Lobatto–Legendre quadrature to be exact in terms of the number of modes for the original expansion for given polynomial orders of the integrand

Polynomial order $N$	Number of quadrature points $Q$
$[u(\xi)]^2 \in P_{2N}$	$Q = [M + 1/2]$
$[u(\xi)]^3 \in P_{3N}$	$Q = 3M/2$
$[u(\xi)]^4 \in P_{4N}$	$Q = [2M - 1/2]$

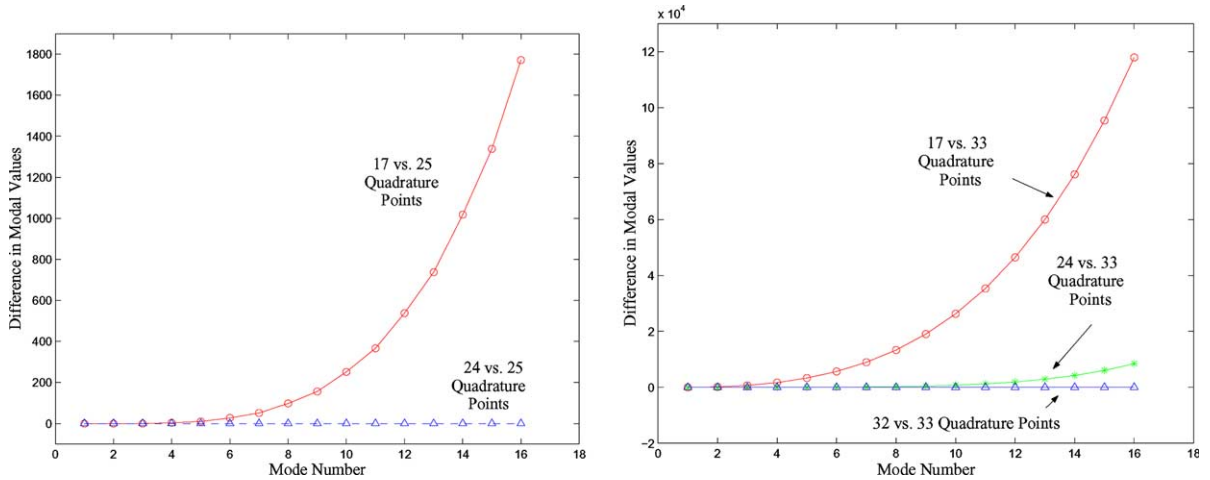


Fig. 1. Comparison of the difference in modal coefficients when different numbers of quadrature points are used. Quadratic non-linearity is shown on the left and cubic non-linearity is shown on the right.

quadrature points as used, then there remain differences in the upper one-third of modes as shown in Fig. 1 (right).

Note that the quadrature rules above for quadratic and cubic non-linearities mimic the de-aliasing rules used for the Fourier method [4]. Although the “rules” appear to give the same result, the rationale behind the rules is slightly different. The goal of polynomial de-aliasing is to find the necessary number of quadrature points so that the computation of the variation form of the non-linear terms is exact.

### 3. Super-collocation for the Burgers equation

To further test the integration of the non-linear terms, we chose to solve the viscous Burgers equation on the interval  $[-1, 1]$

$$\frac{\partial u}{\partial t} + \frac{1}{2} \frac{\partial u^2}{\partial x} = \nu \frac{\partial^2}{\partial x^2} u \quad (1)$$

with initial condition  $u(x) = -\sin(\pi x)$  and periodic boundary conditions using both a *continuous Galerkin* and a *discontinuous Galerkin* method. The specific cases considered are discussed below.

#### 3.1. Continuous Galerkin method

In this example, we present the continuous Galerkin ( $C^0$ ) solution of the viscous Burgers equation with  $\nu = 10^{-5}$ ; Gauss–Lobatto–Legendre points are used for each element. The simulation parameters are presented in Table 3; we draw your attention to the fact that five equally spaced spectral elements were used, each of which contained  $M = 16$  modes in its polynomial expansion. The number of elements and the element spacing were chosen so that the steep gradient in the solution occurs in the middle of an element and not at an element interface. This choice forces the *middle* element to accommodate the steep gradient by involving most of the modes in its elemental polynomial expansion, hence making it a prime candidate for aliasing problems. The rationale for this example is to test whether the solution of a system with a small amount of viscosity is sufficient to overcome the “numerical crimes” committed by under-integrating the non-linear terms, and hence render the solution stable.

Table 3  
Parameters used for the results presented in Fig. 2

Parameters	Values
Method	Continuous Galerkin
Number of elements	5
Modes	16
Time integrator	Second order Adams–Bashforth
Final time $T$	0.5
$\Delta t$	0.0001

If  $Q = M + 1 = 17$  quadrature points are used for integrating both the advection and diffusion terms, the solution is unstable. If, however,  $Q = 3M/2 = 24$  quadrature points are used as in Fig. 2 (top), the solution is stable. To verify that indeed the over-integration is only necessary for the advection (non-linear) terms and not the diffusion terms (which, because they are linear, should only require  $M + 1$  points for exact integration), we also computed the solution when  $Q = 24$  points were used for integrating the advection term and  $Q = 17$  points were used for integrating the diffusion term. The result is presented in Fig. 2 (bottom). The difference in the  $L_\infty$  norm of the solution is negligible.

To further extend our understanding of the problems which may arise due to under-integration, we also solved the viscous Burgers equation with  $\nu = 10^{-2}/\pi$  using the continuous Galerkin method. This problem was used as a test problem in [9] for evaluating the effectiveness of different spatial discretizations. As is pointed in that paper, for  $\nu = 10^{-2}/\pi$  the solution develops into a sawtooth wave centered at the origin around the time  $t = 1/\pi$  (an approximation which comes from the inviscid theory for Burgers equation), and the maximum gradient of the solution occurs at approximately  $t = 0.5$ . As in [9], the Cole transformation is used to obtain the exact solution to Eq. (1)

$$u(x, t) = - \frac{\int_{-\infty}^{\infty} \sin(\pi(x - \eta)) f(x - \eta) \exp(-\eta^2/4\nu t) d\eta}{\int_{-\infty}^{\infty} f(x - \eta) \exp(-\eta^2/4\nu t) d\eta}, \tag{2}$$

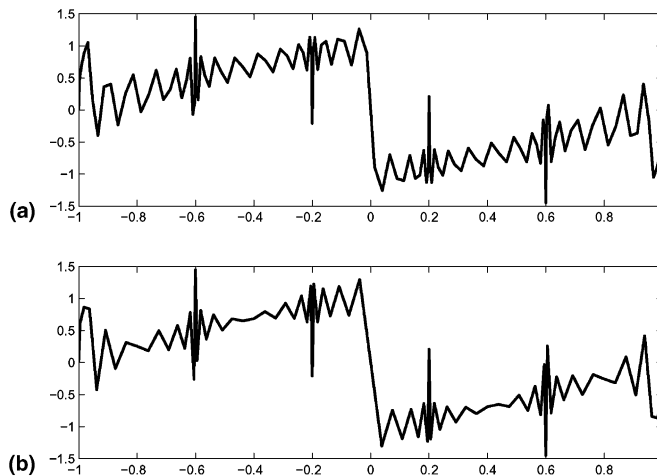


Fig. 2. Solution of the viscous Burgers equation with  $\nu = 10^{-5}$  evaluated at  $T = 0.5$ . (a)  $Q = 24$  quadrature points are used for integrating both the advection and diffusion terms. (b)  $Q = 24$  quadrature points are used for the advection term, and only  $Q = 17$  points are used for the diffusion terms.

where

$$f(y) = \exp(-\cos(\pi y/2\pi v)). \quad (3)$$

In the current study, the convolution operator given in Eq. (2) was computed numerically using Gauss–Hermite integration with up to 30 terms.

Our rationale in this example is to see how much viscosity is necessary to stabilize the solution when under-integration is involved, and to compare solutions against an exact solution. Three cases were examined (and are plotted in Fig. 3):

- (i) Case 1:  $Q = 17$  quadrature points used for integrating both the advection and diffusion terms (top figure).
- (ii) Case 2:  $Q = 24$  quadrature points used for integrating both the advection and diffusion terms (middle figure).
- (iii) Case 3:  $Q = 24$  points used for integrating the advection term and  $Q = 17$  points used for integrating the diffusion term (bottom figure).

In Table 4 we present the error in the discrete  $L_\infty$  norm for the three cases presented above. Observe that both case two and case three show marked improvement over case one. The small discrepancy between case two and case three can be explained by the fact that the discrete (pointwise)  $L_\infty$  norm is taken over the number of points used for the diffusion operator. Hence, in case two more (and different) points were used for the diffusion operator than in both case one and case three. The overall trend, and hence the point of the test, was not affected however.

As is evident from these examples, given sufficiently large viscosity, the solution can be rendered stable. However, since we have an interest in the numerical simulation of high Reynolds number flows, special care must be taken when integrating the non-linear terms, as the viscosity may be insufficient in rendering the solution stable.

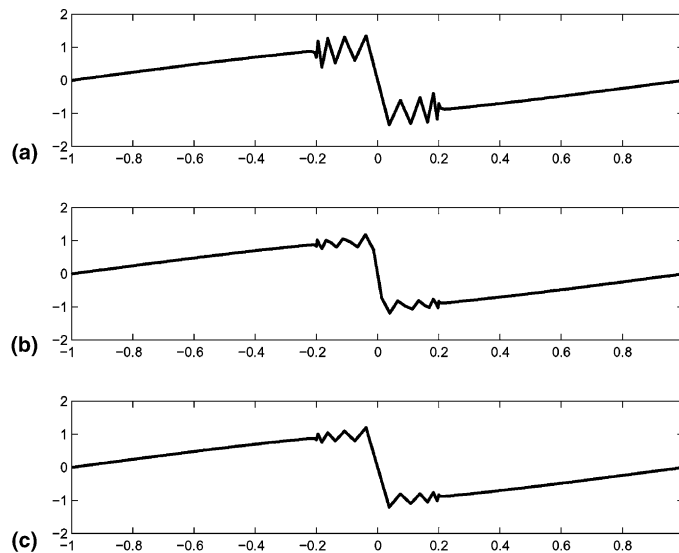


Fig. 3. Solution of the viscous Burgers equation with  $\nu = 10^{-2}/\pi$  evaluated at  $T = 0.5$ . (a)  $Q = 17$  quadrature points are used for integrating both the advection and diffusion terms. (b)  $Q = 24$  quadrature points are used for integrating both the advection and diffusion terms. (c)  $Q = 24$  quadrature points are used for the advection term, and only  $Q = 17$  points are used for the diffusion terms.

Table 4  
Error in the discrete  $L_\infty$  norm for the three cases presented above

Cases	Error in the discrete $L_\infty$ norm
1	0.5090
2	0.2729
3	0.2038

### 3.2. Discontinuous Galerkin method

In order to appreciate the effect of under-integration in the context of a numerical solution obtained using the discontinuous Galerkin method, we consider the *inviscid Burgers equation*, which we discretize using the discontinuous Galerkin method as presented in [8]. The initial condition is  $u(x) = -\sin(\pi x)$ , and five equally spaced elements spanning  $[-1, 1]$  were used, each one having  $M = 16$  modes. Periodic boundary conditions are assumed. The final time  $T$ , the time step and time integrator used were the same as given for the continuous Galerkin case (see Table 3). In Fig. 4, we plot the  $L_2$  norm of the solution versus the number of quadrature points used for numerical integration. When using  $Q = 17, 19$  and  $Q = 21$  points, the solution is unstable. Once the number of quadrature points reaches  $Q = 24$  ( $3/2M$ , where  $M$  is the number of modes), the  $L_2$  norm of the solution does not change. The alternating unstable/stable pattern exhibited for  $Q = 17$  through  $Q = 22$  may be due to the fact that for some elements only the even modes are excited (this issue will be demonstrated below). As the quadrature order is increased, different mode combinations are integrated properly; only after a sufficient number of quadrature points is used ( $Q > 21$ ) does the solution remain stable for all  $Q$ . The point of this example is to demonstrate that some stabilizing effects can be obtained by using only a few additional quadrature points (as first observed in [8]). However, only after the proper number of over-integrated points are employed does the computation solution present consistent behavior (in this case measured as the  $L_2$  norm of the solution). The discrepancy from unity for the  $L_2$  norm of the solution is due to the dissipation properties of the advective flux employed [10,11].

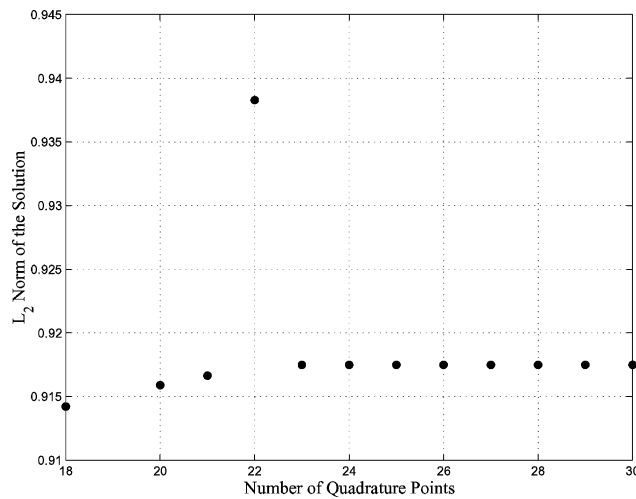


Fig. 4. Solution of the inviscid Burgers equation evaluated at  $T = 0.5$ . Five equal spaced elements were used with 16 modes in each element. On the ordinate we plot the  $L_2$  norm of the solution, and on the abscissa we plot the number of quadrature points used for numerical integration. The solution is unstable for  $Q = 17, 19$  and  $21$ . Observe that after  $Q = 24$  points, the  $L_2$  norm of the solution does not change.

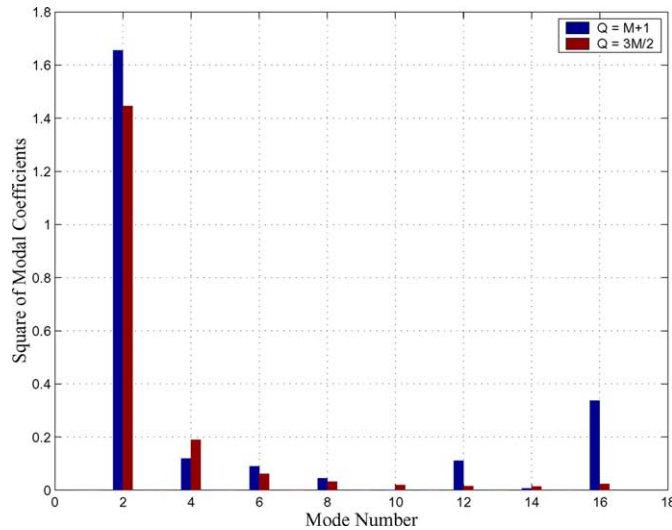


Fig. 5. Modal coefficients in the middle element of the inviscid Burgers solution at time  $T = 0.35$ . Over-integration using  $Q = 3M/2$  quadrature points leads to a stable solution unlike the  $Q = M + 1$  case. For each mode number, the bar on the left denotes  $Q = M + 1$  while the bar on the right denotes  $Q = 3M/2$ .

We can analyze this behavior by examining the energy in the modes (denoted by the square of the modal values) within the element that contains the jump in the inviscid Burgers solution. The modes were extracted at time  $T = 0.35$ , after the shock has formed (at time  $1/\pi$ ) and prior to the solution becoming unstable. In Fig. 5, we plot the square of the modal coefficients versus the mode number. Due to the symmetry of the element placement, only even number modes were excited.

The case corresponding to using  $Q = 17$  quadrature points will become unstable by time  $T = 0.5$ . If a  $3/2M$  rule is used, yielding  $Q = 24$  points, the solution is stable, and the energy is much less than when the non-linear terms are under-integrated. Hence when no over-integration is used, the energy in the highest modes grows, indicating an aliasing error. When over-integration is applied, however, the modal coefficients of the inviscid Burgers solution converge monotonically to zero leading to a stable simulation unlike the untreated simulation. This plot shows vividly the effects of aliasing when under-integration of the non-linear terms is performed.

#### 4. Polynomial de-aliasing in flow simulations

We now present three direct numerical simulation results which demonstrate the effect of over-integration. First, we present incompressible flow results for a transitional and turbulent state in a triangular duct demonstrating the effect of polynomial aliasing and its correction through over-integration. We then present results for incompressible flow in a channel at  $Re_\tau = 395$  in which over-integration is used to stabilize a coarse resolution simulation. Lastly we present results for compressible flow around a pitching airfoil at  $Re = 45,000$  in which over-integration is again used for stabilization of the solution.

##### 4.1. Transition and turbulence in a triangular duct

We demonstrate the effect of under-integration and associated aliasing errors by simulating transition to turbulence of incompressible flow in a duct with its cross-section being an equilateral triangle. The laminar

fully developed solution is known analytically. We introduce some random disturbances in the flow, and we integrate in time until these disturbances start decaying or growing in time. The incompressible fluid version of the spectral/hp element code *Nek5000* [12] which is based on the continuous Galerkin method was employed for these simulations. All simulations were performed in the domain shown in Fig. 6 with the cross-section discretized using one triangular element only and 16 Fourier modes (32 collocation points) in the streamwise (homogeneous) direction. A duct length of three units was used. The Reynolds number is defined as  $Re = UD_e/\nu$ , where  $U$  is the average velocity and  $D_e$  is the equivalent (hydraulic) diameter. For  $Re \leq 500$  all disturbances decay, but for  $Re = 1250$  the flow goes through transition, and a turbulent state is sustained. Typical results are shown in Fig. 6.

We have performed three simulations at  $Re = 1250$  corresponding to three different combinations of polynomial order ( $M$ ) and quadrature order ( $Q$ ). In the first one, shown in Fig. 7(a), we consider the case where  $Q = M + 1$ , where  $M = 16$ . The forces on the three walls of the duct are plotted as a function of time. From symmetry considerations, we expect that the statistical averages of the three forces are identical, but obviously the symmetry in the mean is not preserved here. In Fig. 7(b) we plot the forces for the case with  $Q = 2M$ , and in Fig. 7(c) the case with  $Q = 3M/2$ . We have verified that in both cases the same statistical force average is obtained, consistent with the analysis presented above for handling under-integration induced errors. We have also run a simulation in which  $M = 21$  modes were used with no over-integration, and statistically identical results are obtained compared to the  $M = 16$  case with over-integration. This further supports the claim that when sufficient resolution is used, the effect of aliasing errors are minimized. However, in marginally resolved or under-resolved simulations, aliasing errors may significantly pollute the solution.

In Table 5, we present the mean shear force calculated for each of the walls. Statistical averaging was started 40 convective units (over 13 duct lengths) after the initial perturbation period of 10 convective units; statistical averages were taken over 150 convective units (50 duct lengths).

#### 4.2. Coarse resolution channel simulation at $Re_\tau = 395$

The effectiveness of spectral vanishing viscosity (SVV) in simulations of turbulent flows using low resolution has been demonstrated in [13,14]. Here, we revisit the problem presented in [13] of simulating turbulent channel flow at  $Re_\tau = 395$  using only over-integration and no SVV filtering. Using the incompressible version of the spectral/hp element code *Nek5000*, channel flow at  $Re_\tau = 395$  is simulated with

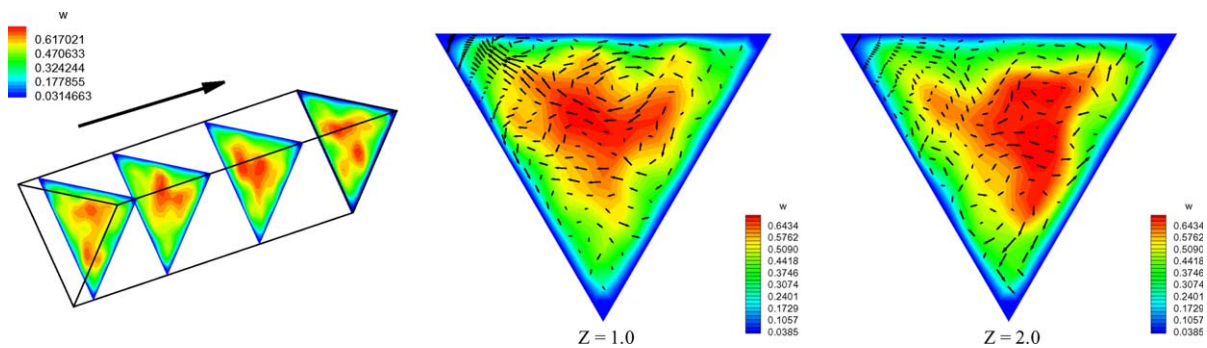


Fig. 6. Duct flow domain: the cross-section is an equilateral triangle and the streamwise length is three times the triangle edge. On the left we show a frame of the entire domain with flood contour cut-planes of the fluid velocity in the streamwise ( $w$ ) direction. In the center and on the right we present flood contour cut-planes of the fluid velocity in the streamwise ( $w$ ) direction with arrows denoting the velocity in the crossflow ( $u, v$ ) directions at  $z = 1$  and  $z = 2$ , respectively.

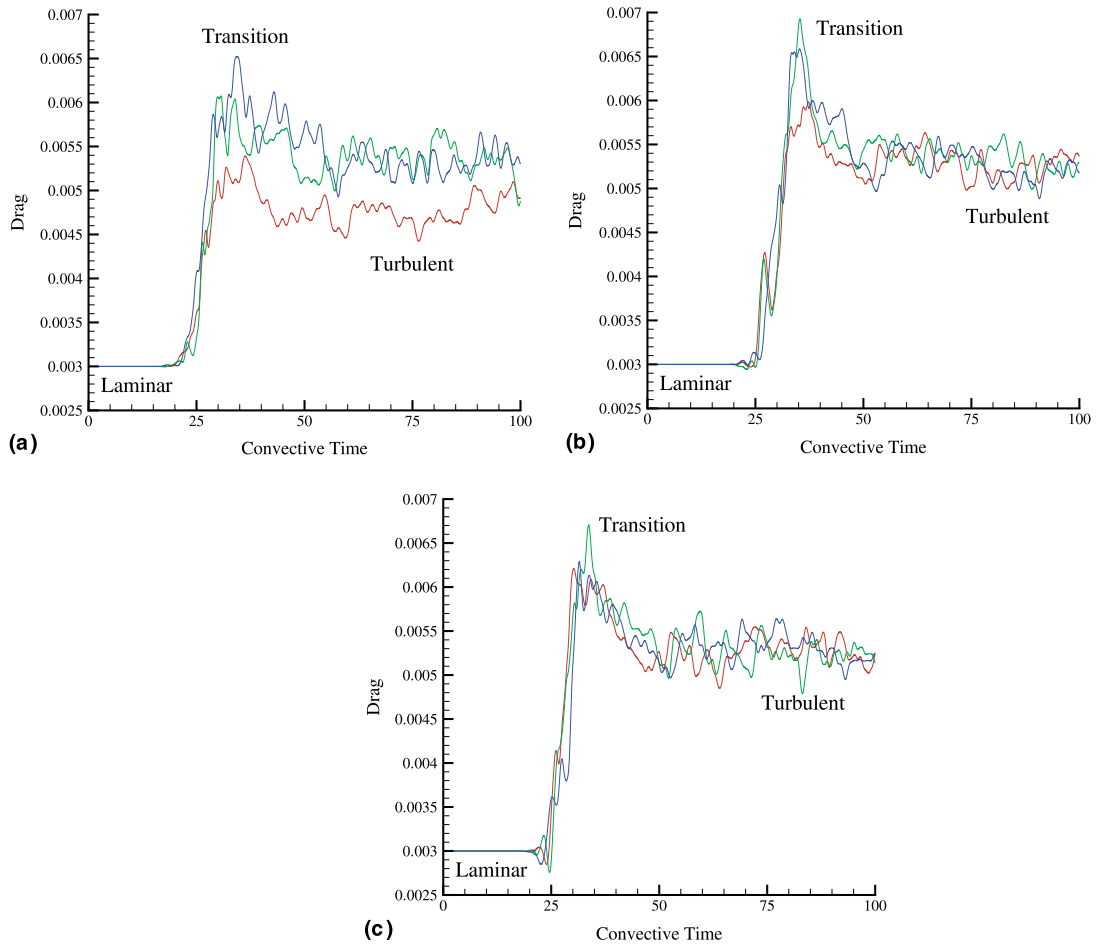


Fig. 7. Wall shear forces as a function of time for: (a)  $Q = M + 1$ ; (b)  $Q = 2M$ ; (c)  $Q = 3M/2$ .

Table 5  
Mean shear forces on each wall versus the quadrature order employed

Quadrature order	Wall 1	Wall 2	Wall 3
$M + 1$	0.0048	0.0054	0.0054
$(3/2)M$	0.0053	0.0053	0.0053
$2M$	0.0053	0.0053	0.0053

periodic boundary conditions in the streamwise and spanwise directions following the benchmark solutions of Moser et al. [15]. The mesh used here is the same as in [13]. Specifically, a computational domain of  $2\pi\delta \times 3 \times 2$  was used in the streamwise, spanwise and wall-normal directions, respectively. The spectral element mesh has 25 elements (see Fig. 8) in the crossflow plane, with a polynomial order of  $N = 20$  (i.e.,  $M = 21$  modes per polynomial direction). In the homogeneous streamwise direction, 64 Fourier modes were used with a  $3/2$  de-aliasing rule applied. The resulting *average* resolution is  $\Delta x^+ = 10$ ,  $\Delta z^+ = 6.5$ , and  $\Delta y^+ = 11.6$  at the centerline.

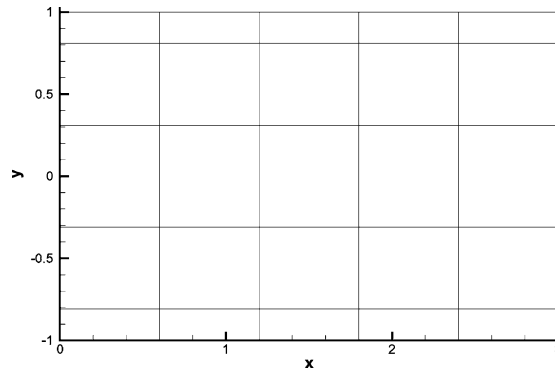


Fig. 8. Two-dimensional slice (crossflow plane) for turbulent channel flow at  $Re_\tau = 395$ .

As was remarked in [13], at this low resolution, the untreated (non-SVV, no over-integration) DNS solution eventually goes unstable. Previously, only through the use of SVV could a stable computation at this coarse resolution be realized. We found, however, that over-integration with a  $3M/2$  quadrature rule achieves asymptotic stability of the numerical solution as well.

In Fig. 9 we present the turbulent intensities in the streamwise, spanwise, and wall-normal directions for our low-resolution, over-integrated solution. We compare our simulation results against the benchmark DNS computation of [15] at the same Reynolds numbers. Even after long time integration, the over-integrated simulation remains stable. Comparing the solution to that of Moser et al., we see that turbulent intensities exhibit signs of under-resolution, which we expect given the coarse resolution used.

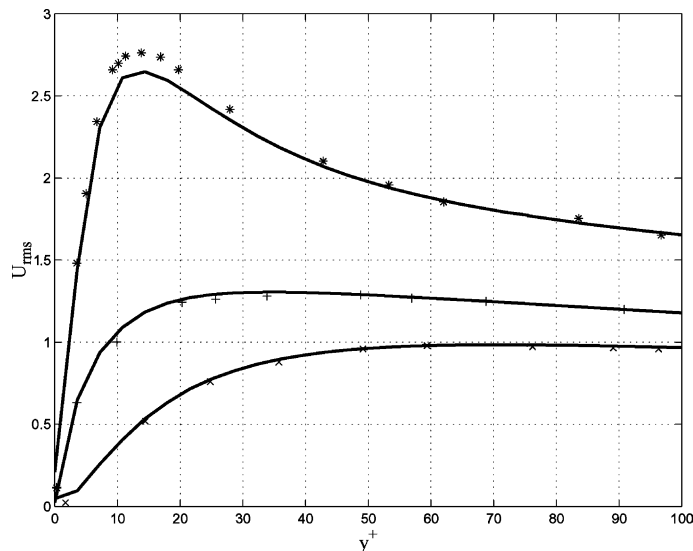


Fig. 9. Turbulence intensities for the turbulent channel flow. The symbols correspond to the benchmark solutions of Moser et al. [15] (\* denotes the streamwise component; + denotes the spanwise component; and × denotes the wall-normal component). The solid-line corresponds to the under-resolved DNS with over-integration.

### 4.3. Two-dimensional flow around a pitching airfoil

To demonstrate the effect of over-integration when using the discontinuous Galerkin method, we examine the laminar compressible flow around a rapidly pitching NACA 0015 airfoil and compare lift coefficients against the established computational results of Visbal and Shang [16]. For these computations, the compressible version of the spectral/*hp* element code *NekTar* [8] was used. The NACA 0015 airfoil is pitching upwards about a fixed axis at a constant rate from zero incidence to a maximum angle of attack of approximately  $60^\circ$ . The pivot axis location is at  $1/4$  of the chord measured from the leading edge. The temporal variation of the pitch given in [16] is

$$\Omega(t) = \Omega_0[1 - e^{-4.6t/t_0}], \quad t \geq 0, \quad (4)$$

where  $t_0$  denotes the time elapsed for the airfoil to reach 99% of its final pitch rate  $\Omega_0$ . Here, the non-dimensional values are  $t_0^* = 0.5$  and  $\Omega_0^* = 0.2$  based on the chord length and free stream velocity. As initial condition the computed field at  $0^\circ$  angle of attack is used. The Mach number is 0.2 and the chord Reynolds number is 45,000.

In [16] a similar simulation was performed using a grid fixed to the airfoil by employing an appropriate transformation and discretizing the modified compressible Navier–Stokes equations using the implicit approximate factorization of Beam and Warming [17]. A typical grid used in [16] involved  $203 \times 101$  points. Although accurate, this approach is not general for moving domains and cannot be used, for example, in simulating multi-body dynamics.

To demonstrate the effectiveness of over-integration, we present two comparisons. First, we present results in which we compare over-integration and SVV. Second, we present a comparison of high-resolution versus low-resolution over-integrated results.

#### 4.3.1. SVV comparison

The purpose of this study is to compare over-integration and SVV [13,14]. In the present study, we employ the ALE formulation on the domain shown in Fig. 10. The computational mesh used for this simulation consisted of 912 quadrilateral elements; the full domain and local tessellation are shown in Fig. 10. Polynomials of degree nine were used for both over-integrated and SVV computations.

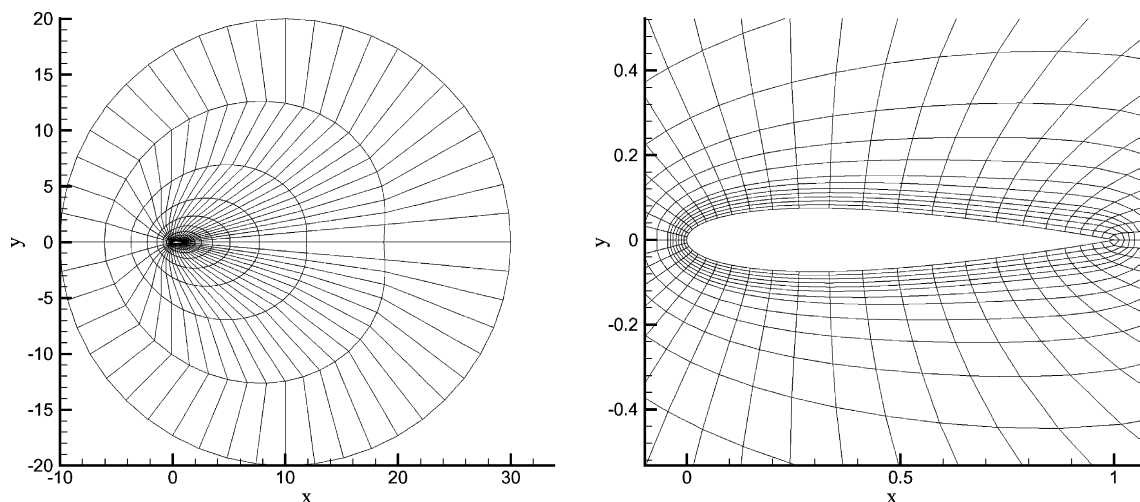


Fig. 10. Full domain (left) and local tessellation (right) for the simulation around the NACA 0015 pitching airfoil. All dimensions are in units of chord length.

Without the use of over-integration or SVV, this computation goes unstable. The goal of this experiment is two-fold: first, to verify if over-integration stabilizes the solution, and second, to see if SVV can replace over-integration as a means of stabilizing the computation.

In Fig. 11 we present the coefficient of lift  $C_L$  for the over-integrated (dashed line) and SVV (solid line) cases. We also present a comparison to the experimental and computational results presented in [16]. We observe that over-integration does indeed stabilize the solution throughout the entire time integration, whereas the SVV solution eventually goes unstable at an angle of attack equal to  $\alpha = 21.7816$ . We note that the coefficient of lift as we have computed contains many more wiggles than that of the computation of Visbal. We attribute this to the fact that we are using a much higher resolution than the original computation of Visbal, and hence are capturing finer details of the shedding dynamics. To illustrate this dynamics we present in Fig. 12 density contours of the over-integrated results for three different angles of attack,  $\alpha = 10.4$  (left),  $\alpha = 26.1$  (center), and  $\alpha = 52.2$  (right).

#### 4.3.2. Resolution comparison

The purpose of this study is to compare over-integration at high-resolution versus low-resolution. In the present study, we employ the ALE formulation on the domain shown in Fig. 13. The computational mesh

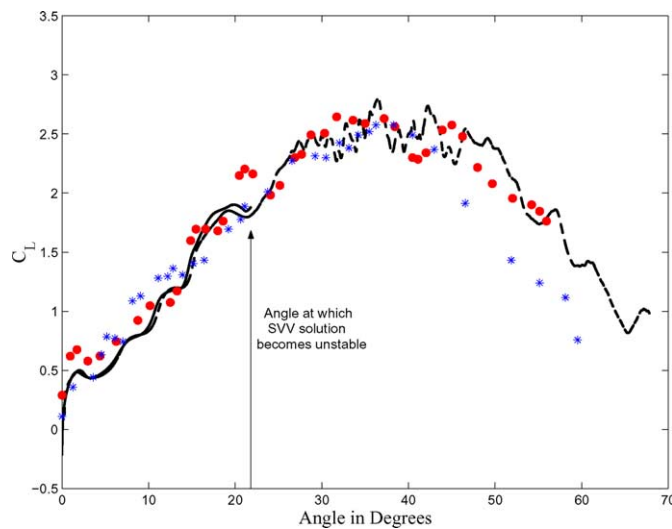


Fig. 11. Comparison of the lift coefficient  $C_L$  versus angle of attack in degrees for SVV (solid), over-integrated (dashed), and the computational (circle) and experimental (asterisk) results presented in [16].



Fig. 12. Density contours for angles of attack  $\alpha = 10.4$  (left),  $\alpha = 26.1$  (center), and  $\alpha = 52.2$  (right).

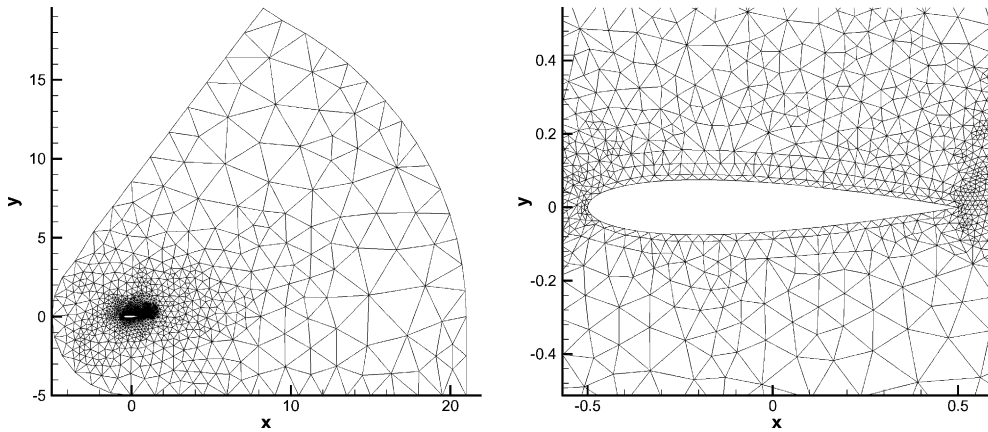


Fig. 13. Full domain (left) and local triangulization (right) for the simulation around the NACA 0015 pitching airfoil. All dimensions are in units of chord length.

used for this simulation consisted of 3838 triangular elements; the full domain and local triangulation are shown in Fig. 13.

For this study three cases (labeled A–C) were computed. All three cases used the same triangulation, however different polynomial orders and number of quadrature points were used. The parameters for the three cases are presented in Table 6.

Table 6  
Polynomial order per tensor product direction and number of quadrature points per direction used for cases A–C

Cases	Polynomial order ( $M$ )	Number of quadrature points ( $Q$ )
A	Ninth order	20
B	Second order	6
C	Third order	8

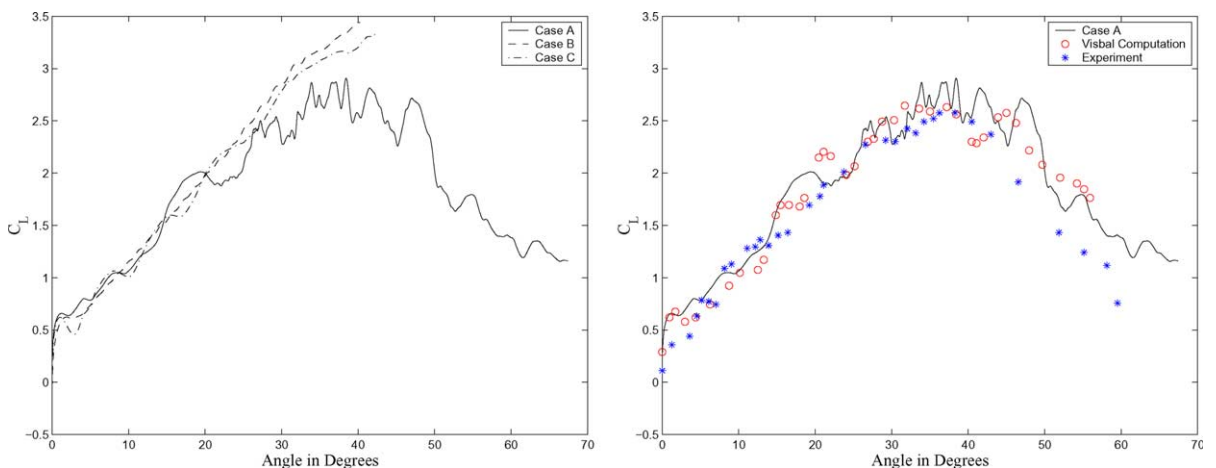


Fig. 14. Comparison of the lift coefficient  $C_L$  versus angle of attack in degrees for cases A–C (left) and case A compared with the computational and experimental results presented in [16] (right).

In Fig. 14 we present the coefficient of lift  $C_L$  for cases A–C with comparison to the experimental and computational results presented in [16]. Case A is our control case with high polynomial order and is stable both with and without over-integration. The coefficient of lift differs only slightly between the over-integrated and non-over-integrated cases for this high-order simulation. Cases B and C are both unstable if over-integration is not employed. Appropriate over-integration leads to a stable computation until an angle of attack of approximately  $37^\circ$  where both computations finally go unstable. Even with the extremely low resolution of these two cases, the computational results capture the general trend of the control case, only starting to deviate at high angles of attack prior to going unstable. Also observe that increasing the polynomial order draws the computational result closer to the control case indicating a p-type convergence to the control solution.

## 5. Summary and discussion

We have presented a mathematical rationale and computational examples to support the use of over-integration as a means of de-aliasing the discrete form of non-linear terms when using polynomial methods on non-uniform grids. Based on the above analysis and results as well as other similar results, we can state the following semi-empirical rules:

*De-aliasing rule 1:* For quadratic non-linearities employing super-collocation with  $3/2M$  grid (quadrature) points per direction, where  $M$  is the number of modes in one direction of the tensor product expansion, followed by a Galerkin projection leads to a de-aliased turbulence simulation on non-uniform grids.

*De-aliasing rule 2:* For cubic non-linearities employing super-collocation with  $2M$  grid (quadrature) points per direction, where  $M$  is the number of modes in one direction of the tensor product expansion, followed by a Galerkin projection leads to a de-aliased simulation on non-uniform grids.

The implementation of over-integration is straight-forward, requiring only an implementation which allows the number of quadrature points used for the Galerkin projections to be de-coupled from the number of modes employed. The primary drawback of over-integration is that the computational cost is increased. The computational cost of the tensor-product quadrature rules for multi-dimensional elements still asymptotically scales the same as before, however, the coefficient in front is much larger due to the additional super-collocation.

It has been proposed that polynomial filtering [18] or SVV [13] may provide a more computationally efficient means of removing the effects of polynomial aliasing. Such filtering techniques have been successfully employed to stabilize spectral element polynomial methods [6,19,20]. These methodologies, however, do not directly address the cause of the aliasing error, but merely provide a mechanism for dissipating the aliasing energy that arises due to the numerical crimes committed.

Having obtained the results presented here, it is desirable in the future to develop a rigorous theory that provides justification and insight into both the stability and accuracy enhancements demonstrated with the proposed algorithms.

## Acknowledgements

We would like to thank Profs. Jan Hesthaven and David Gottlieb for their helpful comments. This work was supported by AFOSR and ONR, and computations were done on the the SGI Origin 2000 at NCSA (University of Illinois, Urbana-Champaign) and on the IBM SP at TCASCV (Brown University).

## References

- [1] G.E. Karniadakis, S.J. Sherwin, *Spectral/hp Element Methods for CFD*, Oxford University Press, Oxford, 1999.
- [2] B. Cockburn, S. Hou, C.-W. Shu, The Runge–Kutta local projection discontinuous Galerkin finite element method for conservation laws IV: the multidimensional case, *Math. Comput.* 54 (1990) 545–581.
- [3] C. Canuto, A. Quarteroni, Approximation results for orthogonal polynomials in Sobolev spaces, *Math. Comput.* 38 (157) (1982) 67–86.
- [4] C. Canuto, M.Y. Hussaini, A. Quarteroni, T.A. Zang, *Spectral Methods in Fluid Mechanics*, Springer, New York, 1987.
- [5] Y. Maday, E.M. Rønquist, Optimal error analysis of spectral methods with emphasis on non-constant coefficients and deformed geometries, *Comp. Meth. Appl. Mech. Eng.* 80 (1990) 91–115.
- [6] M.O. Deville, E.H. Mund, P.F. Fischer, *High Order Methods for Incompressible Fluid Flow*, Cambridge University Press, Cambridge, 2002.
- [7] I. Lomtev, A discontinuous Galerkin method for the compressible Navier–Stokes equations in stationary and moving domains, PhD Thesis, Applied Mathematics, Brown University, 1999.
- [8] I. Lomtev, R.M. Kirby, G.E. Karniadakis, A discontinuous Galerkin ALE method for compressible viscous flows in moving domains, *J. Comp. Phys.* 155 (1999) 128–159.
- [9] C. Basdevant, M. Deville, P. Haldenwang, J.M. Lacroix, J. Ouazzani, R. Peyret, P. Orlandi, A.T. Patera, Spectral and finite difference solutions of the Burgers equation, *Comput. Fluids* 14 (1) (1986) 23–41.
- [10] S.J. Sherwin, Dispersion analysis of the continuous and discontinuous Galerkin formulations, in: B. Cockburn, G.E. Karniadakis, C.-W. Shu (Eds.), *Discontinuous Galerkin Methods: Theory, Computation and Applications*, Springer, Berlin, 2000.
- [11] F.Q. Hu, M.Y. Hussaini, P. Rasetarinera, An analysis of the discontinuous Galerkin method for wave propagation problems, *J. Comp. Phys.* 151 (1999) 921–946.
- [12] R.M. Kirby, T.C. Warburton, S.J. Sherwin, A. Beskok, G.E. Karniadakis, The *Nek5000* code: dynamic simulations without remeshing, In: *Proc. of the 2nd International Symposium on Computational Technologies for Fluid/Thermal/Chemical Systems with Industrial Applications*, ASME PVP Division, vol. 397, 1999.
- [13] G.-S. Karamanos, G.E. Karniadakis, A spectral vanishing viscosity method for large-eddy simulations, *J. Comp. Phys.* 162 (2000) 22.
- [14] R.M. Kirby, G.E. Karniadakis, Coarse resolution turbulence simulations with spectral vanishing viscosity – large-eddy simulations (SVV–LES), *J. Fluid Eng.* 124 (4) (2002) 886–891.
- [15] R.D. Moser, J. Kim, N.N. Mansour, Direct numerical simulation of turbulent channel flows up to  $Re_\tau = 590$ , *Phys. Fluids* 11 (4) (1999) 943–945.
- [16] M.R. Visbal, J.S. Shang, Investigation of the flow structure around a rapidly pitching airfoil, *AIAA J.* 27 (8) (1989) 1044–1051.
- [17] R. Beam, R. Warming, An implicit factored scheme for the compressible Navier–Stokes equations, *AIAA J.* 16 (1978) 393–402.
- [18] D. Gottlieb, J.S. Hesthaven, Spectral methods for hyperbolic problems, *J. Comput. Appl. Math.* 128 (1–2) (2001) 83–131.
- [19] J.S. Mullen, P.F. Fischer, Filtering techniques for complex geometry fluid flows, *Commun. Numer. Meth. Eng.* 15 (1999) 9–18.
- [20] P.F. Fischer, J.S. Mullen, Filter-based stabilization of spectral element methods, in: *Comptes Rendus de l’Académie des sciences Paris*, t. 332, – Srie I – Analyse numérique, 2001, pp. 265–270.